Hindawi Publishing Corporation
Journal of Nanomaterials
Volume 2007, Article ID 27437, 16 pages
doi:10.1155/2007/27437

Research Article

Broadband Ferromagnetic Resonance Measurements in Ni/ZnO and Niγ-Fe_2O_3 Nanocomposites

Vincent Castel,[1] Jamal Ben Youssef,[2] and Christian Brosseau[1,3]

[1] *Laboratoire d'Electronique et Systèmes de Télécommunications (UMR CNRS 6165), Université de Bretagne Occidentale, CS 93837, 6 avenue Le Gorgeu, 29238 Brest Cedex 3, France*
[2] *Laboratoire de Magnétisme de Bretagne (FRE CNRS 2697), Université de Bretagne Occidentale, CS 93837, 6 avenue Le Gorgeu, 29238 Brest Cedex 3, France*
[3] *Département de Physique, Université de Bretagne Occidentale, CS 93837, 6 avenue Le Gorgeu, 29238 Brest Cedex 3, France*

Received 16 February 2007; Accepted 27 June 2007

Recommended by Donald A. Bansleben

A comparative study at the ambient temperature of the ferromagnetic resonance (FMR) spectra of Ni/ZnO and Ni/γ-Fe_2O_3 nanocomposites (NCs) is reported. A microstrip transmission line technique was used to measure the FMR profiles and linewidths in the 8–24 GHz frequency range. The samples were placed at the center of a microstrip line where the derivative of the absorbed power was measured using a standard ac field modulation technique (10 Oe amplitude) and lock-in detection. The analysis of the FMR spectra can be interpreted as arising from aggregates of magnetic nanoparticles, each of which resonates in an effective magnetic field composed of the applied field, the average (magnetostatic) dipolar field, and the randomly oriented magnetic anisotropy field. It is found that frequency and applied magnetic field strongly influence the lineshape of the FMR spectra. Two observations are identified within the FMR spectra. On the one hand, the resonance field increased linearly with frequency as expected from uniform mode theory and yielded a Landé g factor in the range 1.48–2.05. On the other hand, there is no clear correlation between FMR linewidths and frequency. Inhomogeneity-based line-broadening mechanisms, due to the damping of surface/interface effects and interparticle interaction, affect the FMR effective linewidth.

1. INTRODUCTION

The recent emphasis on nanomaterials for various applications related to spintronics [1, 2], magnetic recording media [3], and magneto-optics [4, 5] has generated considerable interest in several magnetic metal-dielectric systems which have previously received very little attention. There are many instances in which we would like to control the microwave properties of nanocomposites (NCs), selecting from more than one possible magnetic component by adjusting for example parameters of exchange interaction between the individual constituents or, the magnetization-polarization coupling in multiferroic oxides through product property [6–10]. The required coupling between polarization and magnetization is difficult but has been achieved in a number of systems [11–14]. Recently, several approaches to reach this "magnetoelectricity" at microwave frequencies have been suggested and experimentally observed [2, 12, 13]. In the sub-100-nm regime, magnetic particles are single domain, that is, the size of the system is smaller than the exchange correlation length, but the particles eventually form aggregates and apart from the dipolar interaction between the nanoparticles, other types of interactions, for example, intracluster exchange, may also become relevant. The magnetic properties of nanophases are determined both by the behavior of particles and by the spatial distribution of the aggregates which defines the magnetostatic interactions between them. The ability to probe magnetoelectric coupling on the nanoscale in NCs will open a new opportunity to develop novel high-frequency soft magnetic materials and pave the way for advances in nanoelectronics systems. A key feature of these approaches is the use of core-shell structures in which the metal nanograins are insulated by insulating layers, thus the conductivity of the system will be dramatically decreased, leading to a significantly reduced eddy current loss, while the coupling strength between neighboring magnetic aggregates can overcome the anisotropy and demagnetizing effect.

As part of a large effort to quantitatively model the electromagnetic transport properties in nanostructures, we have recently investigated on the microwave properties of NCs

Table 1: Selected physical properties of the powders investigated in this study.

Powder	ZnO	γ-Fe_2O_3	Ni
Average particle size[(a),(b),(c)]	49 nm	23 nm	35 nm
Powder color	White	Brown	Gray
Specific surface area bet (m^2g^{-1})	22	51	15.6
Morphology	Elongated	Nearly spherical, faceted	Spherical
Crystal phase	Wurtzite	Maghemite (cubic spinel)	Fm3m (225) ccp
Density[(a)] ($g\,cm^{-3}$)	5.6	5.2	8.9

[(a)] From manufacturer product literature.
[(b)] Determined from specific surface area.
[(c)] Checked by TEM images.

containing Ni, Co, ZnO, and γ-Fe_2O_3 nanoparticles [15–23]. For these epoxy-coated particles, the distance of closest approach between particles is expected to be large enough for the interactions to have mainly a magnetostatic character [20]. Neither widely-used phenomenological models, nor ab initio effective medium theories (EMTs) are entirely successful in describing all experimental findings concerning the electromagnetic behavior of NCs. This is mainly due to the absence of finite-size and surface effects in these modeling approaches; see, for example, [16–20]. More and more evidence, coming from various researchers employing a panoply of techniques, points to the fact that electromagnetic wave transport, polarization, and magnetization mechanisms in NCs differ from those in bulk samples. Theoretical interest is also motivated by the suggestion that surface magnetic interactions and surface disorder can greatly enhance the effective magnetic properties of nanostructures, for example, coercivity as a consequence of the reduced crystal symmetry near the surface originating from the finite size and possible existence of surface disorder [24–28]. In particular, the set of compounds Ni/γ-Fe_2O_3 and Ni/ZnO have proven fertile to study in order to examine the interplay between magnetic metal and semiconductor oxide as γ-Fe_2O_3 is substituted into the ZnO member [20, 22], which has been seen to occur in a wide variety of granular nanostructures. These nanostructures provide an ideal playground to experimentally investigate some fundamental phenomena connected with interparticle interactions because the specific surface area of γ-Fe_2O_3 nanoparticles is more than three times that of Ni (see Table 1) causing the magnetic boundaries to strongly interact. The controllability in these systems allows a clean study of much complicated physics in a controllable fashion. Indeed, due to the large ratio of surface area to volume in nanosized objects, the behavior of surfaces and interfaces becomes a prominent factor controlling the physical and chemical properties of nanostructured materials. Reasons for this are the confinement of electrons in nanometric dimensions that gives rise to changes in the electronic distribution and thus in the optical, electromagnetic, transport, and so forth, properties and to the surface effects.

A number of experimental techniques are currently being deployed in an effort to understand the dynamic magnetic properties of individual and aggregates of nanoparticles. In this regard, the ferromagnetic resonance (FMR) investigation of magnetic nanomaterials and NCs has received considerable attention over the years [21, 29–33]. FMR spectra, as observed in microwave spectroscopy, are a direct manifestation of the forces that determine the dynamical properties of magnetic materials [34]. The correct interpretation of FMR fundamentals can lead to an evaluation of the effective ferromagnetic resonance frequency ω_{res} and Gilbert damping coefficient α which describe the details of the gyroscopic precession of the magnetization. However, the satisfactory characterization of the FMR characteristics in granular nanostructures has proved to be a challenge. Clearly, there remain fundamental questions about how the microwave magnetic response under magnetic fields, of granular heterostructures in which the constituents can exhibit product properties, can bring information on the role of intergranular exchange effect. The fundamental questions can be stated more generally as: what is the structure of the FMR line (single Lorentzian or composite lineshape), and what changes are initiated in the FMR line by the choice of the magnetic species, composition, and clustering of nanoparticles? These aspects would be expected to have a profound significance on the observed FMR properties of granular nanostructures. In such experiments, the resonance is probed by sweeping the applied field. The resonance fields provide a measurement of the effective field seen by the uniform precession mode that is excited by a uniform rf field. The effective field, H_{eff}, contains contributions from the external field, the demagnetizing field, the exchange field, the magnetostrictive, and the magnetocrystalline energies. FMR results provide accurate measures of the static properties of magnetic composites, given by anisotropy constants, and the dynamic properties, given by the linewidth ΔH of the resonance which provides information on relaxation processes.

The impetus for this work stems from our recent investigations [21, 23], employing microwave, spin-wave, and magnetic characterizations, of the structure-magnetic permeability and permittivity relationships for granular γ-Fe_2O_3/ZnO NCs. In [21], we found that the FMR linewidth is very sensitive to details of the spatial magnetic inhomogeneities and increases continuously with the volume content of magnetic material. Different mechanisms were considered to explain the FMR linewidth: the intrinsic Gilbert damping, the broadening induced by the magnetic inhomogeneities, and the extrinsic magnetic relaxation. From these measurements, the characteristic intrinsic damping dependent on the selected material and the damping due to surface/interface effects

Table 2: Overview of NCs compositions: f_X denotes the volume fraction of the X species, f_p is the porosity of the samples, and f_{resin} is the volume fraction of resin. The uncertainty on f_X is typically of the order of 5%. Compaction pressure for all composites was $10^7\ \text{Nm}^{-2}$ for two minutes.

Material designation	f_{Ni}	f_{ZnO}	f_p	f_{resin}	$f\,\gamma\text{-Fe}_2\text{O}_3$
nNiZ1	0.49	0.08	0.28	0.15	—
nNiZ2	0.42	0.17	0.27	0.14	—
nNiZ3	0. 38	0.21	0.26	0.15	—
nNiZ4	0.33	0.26	0.25	0.15	—
nNiZ5	0.29	0.30	0.26	0.15	—
nNiZ6	0.25	0.35	0.25	0.15	—
nNiZ7	0.18	0.44	0.23	0.14	—
nNiZ8	0.09	0.54	0.22	0.15	—
nNiZ9	0	0.63	0.21	0.16	—
1-nNiF	0.08	—	0.26	0.13	0.53
2-nNiF	0.17	—	0.25	0.14	0.44
3-nNiF	0.29	—	0.27	0.12	0.32
4-nNiF	0.50	—	0.26	0.15	0.09
5-nNiF	0.04	—	0.26	0.25	0.55

and interparticle interaction were estimated. More specifically, we found that the inhomogeneous linewidth (damping) due to surface/interface effects decreases with diminishing particle size, whereas the homogeneous linewidth (damping) due to interactions increases with increasing volume fraction of magnetic particles (i.e., reducing the separation between neighboring magnetic phases) in the composite.

With these considerations in mind and following the same experimental methodology in the current report we undertook a careful experimental study of the effective FMR mode's dependence and effective magnetization of granular NCs as a function on applied magnetic field and frequency, and composition. Emphasis is placed upon the understanding of properties such as the positions, linewidths, and shapes of the FMR lines. Another motivation for the present work was to look more closely at the similarity between the spectra of Ni/γ-Fe_2O_3 and Ni/ZnO NCs to examine if common magnetization properties exist and how these commonalities may relate to the surface anisotropy contribution to the anisotropy of Ni and γ-Fe_2O_3 nanoparticles.

This paper is divided as follows. We first give a brief reprise of the experimental conditions developed in [21], and details of the materials under study. In Section 3, we present the FMR measurements and discuss the experimental results. The discussion focuses on both the frequency and magnetic field dependences of spectroscopic properties. The comparison of these results to similar analysis in γ-Fe_2O_3/ZnO NCs is also given. Section 4 concludes the paper and indicates the direction of further developments. Certain details related to the experimental results are relegated in a couple of appendices.

2. EXPERIMENTAL PROCEDURES

2.1. Materials and sample preparation

The samples studied herein were prepared by mixing the fine particules of neat Ni, γ-Fe_2O_3, and ZnO with a stable epoxy resin widely used for low temperature experiments (Scotchcast 265) and purchased from 3M. A series of 14 powdered NC samples with volume fraction of resin in the range 12–25% (see Table 2) were prepared. The nanosized powders were obtained from Nanophase Technologies Corp., Burr Ridge, Ill, USA. The powders were used without further purification. NCs of Ni and γ-Fe_2O_3 with Ni volume fractions spanning $0 \leq f_{\text{Ni}} \leq 05$ range were prepared through powder pressing and characterized by conductivity and microwave frequency-domain spectroscopy (complex permittivity and magnetic permeability) [18]. The conductivity measurements indicate that the sample size is always below the skin depth for the entire range of frequencies considered (see Appendix A). Materials with nonzero conductivity display eddy (surface) current losses in addition to the FMR losses. Eddy currents shield the magnetic field from penetrating into the particles. However, following the experimental results and the discussion presented in [18], we expect eddy current contribution to the losses to be negligible. The comparison with repeated measurements and fabrication protocols for these NCs gave a possible systematic error in our volume fraction of phases of no more than 5%. The detailed fabrication procedure to achieve homogeneous composition of the samples has been already described in [16–19]. The morphology and size of the starting powders were determined by transmission electron microscopy (TEM). The purity of the phases was checked by X-ray powder diffraction (XRD) and

the crystallite sizes were determined from the line broadening of the reflections using the Scherrer formulas. The grain sizes determined from analysis of bright field cross-sectional TEM images are consistent with the ones obtained from XRD (see Table 1). The fractional volume of voids (porosity) is deduced from density measurements in conjunction with the known volume fractions of ZnO, Fe_2O_3 (or Ni), and epoxy. Two series of granular NCs will be considered: on the one hand, fine-grained composites composed of polycrystalline ferromagnetic Ni clusters in a nanocrystalline nonmagnetic (ZnO) host, and on the other hand, Ni clusters embedded in a host composed of ferrimagnetic γ-Fe_2O_3 nanoparticles.

2.2. FMR and static magnetization properties

For VSM and FMR characterizations, the sample was cut from the initial piece of composite and polished to the cubic shape of 1 mm thickness, 1 mm length, and 1 mm width. A detailed analysis for the specific choice of these dimensions is contained in Appendix B.

The details of the FMR apparatus and procedure can be found elsewhere [21]. Briefly, FMR measurements, conducted in an in-plane field geometry have been done with a commercial spectrometer at frequencies in the range from 8 GHz to 24 GHz. The samples were placed at the center of a microstrip line where the derivative of the absorbed power was measured using a standard ac field modulation technique (10 Oe amplitude) and lock-in detection (Signal Recovery 7225). The cw microwave source consisted of an Anritsu MG3694B synthesized sweeper. The amplitude of the exciting field is evaluated to be 10 mOe, which corresponds to the linear response regime. The waveguide is characterized by a transmission line of 1 mm width, and a length of 10 mm, which is designed to have 50 Ω impedance. The magnetic field was applied normally to the sample plane and was measured using a Hall probe (Lakeshore 450).

dc magnetization measurements were using a vibrating sample magnetometer (VSM), that allows a field sweep of ±10 kOe. All measurements presented in this research were performed at ambient conditions. It should be noted that M-H patterns from different positions of the sample were collected, denoted hereafter as perpendicular (per), or in-plane, and parallel (par), respectively.

3. EXPERIMENTAL RESULTS AND DISCUSSION

3.1. Magnetization of Ni/ZnO, Ni/γ-Fe_2O_3, and γ-Fe_2O_3/ZnO NCs

Before proceeding to discuss FMR results, a preliminary assessment of the magnetic state of the samples has been done through their magnetization (M) versus field (H) plots at 300 K. Typical hysteretic magnetizations corresponding to the Ni/ZnO (nNiZ8) sample containing 8.9 vol % Ni is shown in Figure 1, for per and par positions, with a sharp increase in magnetization at low fields followed by a linear saturating behavior. Observe that the differences between in-plane and out-of-plane hysteresis loops of the sample are small. To extract some interesting information from the

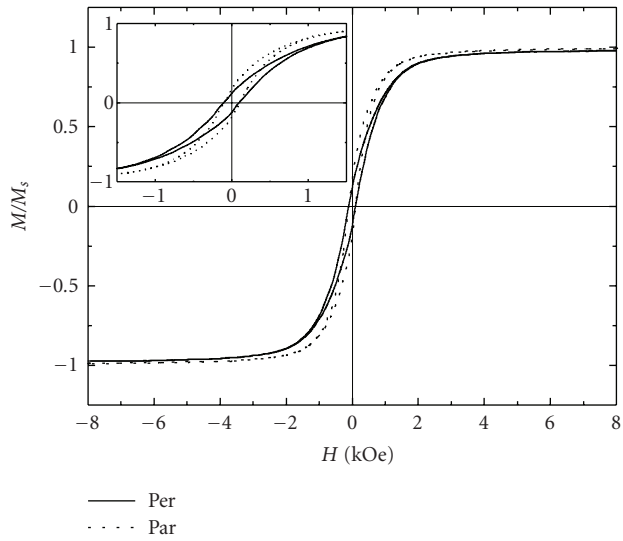

Figure 1: Typical M-H plot of the Ni/ZnO sample (nNiZ8) containing 8.9 vol % of Ni. Room temperature. Inset: an expanded view of the plot clearly showing hysteresis.

in-plane (per) magnetization curves $M(H)$, the saturation magnetization M_s, the coercivity H_c, and the remanent magnetization M_r normalized to M_s (squareness), M_r/M_s, were determined. In Figures 2 and 3, we show the magnitude of M_s, H_c, and M_r/M_s for all samples.

We first compare the effect of the Ni content on the magnetic properties for Ni/ZnO and Ni/γ-Fe_2O_3 NCs. For Ni/ZnO, the M_s values increase linearly (see Figure 2(a)) with increasing Ni content. One feature of interest is illustrated in Figure 2(a) by the solid line which shows that the linear response one would expect for an unmodified Ni phase with a $4\pi M_s$ the same as that obtained for 100 vol %, that is, $4\pi M_s = 6.1$ kG [31–33], cannot be reached: only 75% of this value is found. Hence the static magnetic response observed here cannot be totally explained by the demagnetization process of noninteracting Ni particles. Therefore, this result suggests that some interaction exists between the Ni boundary structures (aggregates). The coercivity H_c (see Figure 2(b)) for Ni/ZnO NCs exceeds the value of Ni/γ-Fe_2O_3 NCs over the entire range of Ni volume fraction explored. This decrease in coercivity for the Ni/ZnO NCs upon increasing the Ni content is not due to the internal porosity since the value of porosity is almost identical for all these kinds of samples (see Table 2). Note that the coercivity observed for the Ni/γ-Fe_2O_3 NCs remains constant in the range of Ni volume fraction explored. While Figure 2(c) shows that the squareness ratio remains fairly constant at an average of 0.06 for the NCs with ZnO, which is significantly much smaller than the value predicted by the Wolfarth model predicting $M_r/M_s = 0.5$ for a random distribution of noninteracting uniaxial single domain particles, with coherent rotation of the magnetization. We believe that this deviation from this ideal value is due to interparticle interactions as a consequence of aggregation within the host matrix. We also observe a slow decrease of this ratio in the case of Ni/γ-Fe_2O_3 NCs for Ni

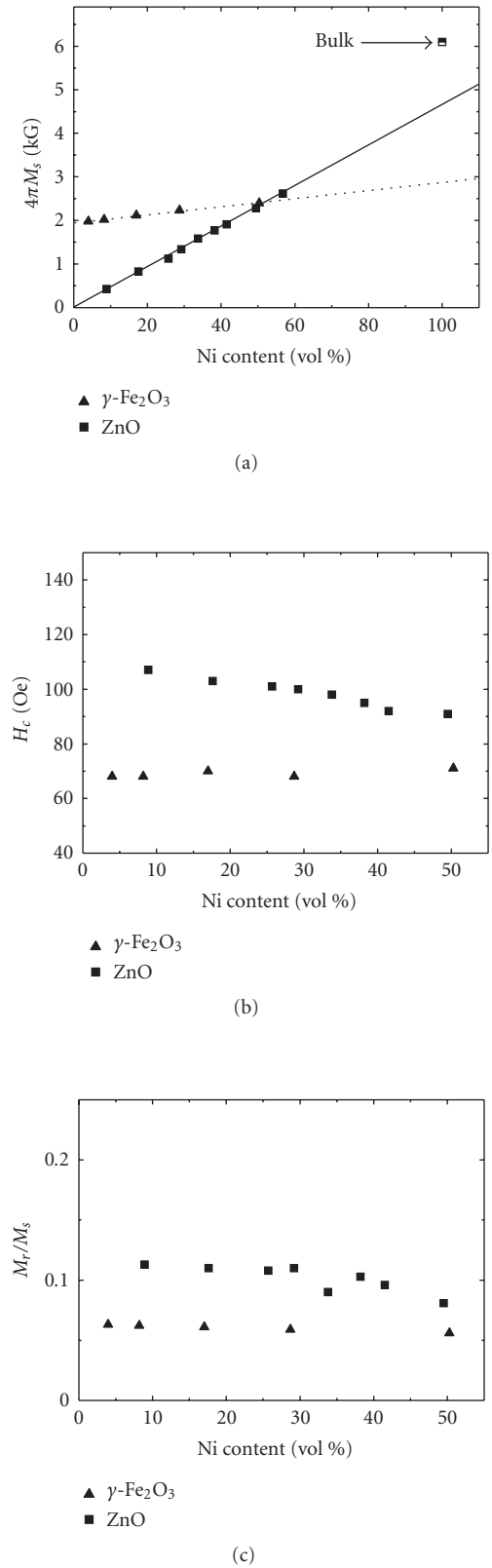

Figure 2: (a) Variation of the saturation magnetization $4\pi M_s$ as a function of Ni content in Ni/ZnO and Ni/γ-Fe_2O_3 samples. Room temperature. Squares (resp., triangles) denote Ni/ZnO (resp., Ni/γ-Fe_2O_3) NCs. (b) Same as in (a) for the coercivity H_c. (c) Same as in (a) for the ratio of remanent magnetization to saturation magnetization (squareness) M_r/M_s.

concentrations above 30%, albeit at a level which exceeds the squareness ratio for the NCs with ZnO.

Further insight into the characteristics of these magnetic states is obtained by comparison with our earlier study [21] of γ-Fe_2O_3/ZnO NCs. For our purpose of comparing M_s, H_c, and M_r/M_s for Ni/γ-Fe_2O_3 and γ-Fe_2O_3/ZnO NCs, the data in Figure 3 reveal that H_c remains constant and that $M_r/M_s \leq 0.15$ over the range of γ-Fe_2O_3 concentration explored. It is also interesting to note that the average saturation magnetization M_s is found to scale linearly with the γ-Fe_2O_3 content, but like the behavior of Ni in the granular ZnO matrix, only 70% of the $4\pi M_s$ value of dense γ-Fe_2O_3, that is, 5.2 kG [31–33], is obtained from the extrapolated value to the 100 vol %. Very recently, Kalarickal et al. [35] found a similar fact in a study of the static magnetic properties of ferrite (nickel zinc)-ferroelectric (barium strontium titanate) composite materials. Although there are some similarities between their samples and our samples, we believe that the differences in interpretation can be explained by different boundaries separating the particles in the samples. The ferrite particles investigated have dimensions of a few micrometers, while the aggregate sizes investigated here have significantly smaller dimensions. In addition, these boundaries differ significantly due to the amorphous (epoxy) interaggregate layer.

3.2. FMR in Ni/ZnO, Ni/γ-Fe_2O_3, and γ-Fe_2O_3/ZnO NCs

Figures 4(a)–4(h) display a series of typical absorption versus field derivative profiles obtained at room temperature, shown in arbitrary units, for five values of the operating frequency for a typical Ni/ZnO NC. Several comments appear warranted after a careful examination of Figure 4. First, we observed that the FMR lineshapes are quite symmetric and undistorted at the lowest Ni volume fractions in the NCs. However, the FMR profiles are more complicated for Ni volume fractions larger than 30%, especially at high frequency. Indeed, one can observe that the derivative profiles of the main resonance are distorted by the presence of higher-order spin-wave modes on the high field side. A detailed examination of the actual FMR profiles shows a secondary peak which appears at the high field tail part of the absorption curve at about 10 kOe (see Figures 4(g) and 4(h)). Second, a weakly resolved line is clearly visible on the low field side at a nominal frequency of 10 GHz. The origin of the weak signal has yet to be elucidated, but it should be remarked that a similar weak signal (at about 500 Oe) was observed in nanogranular films composed of ferromagnetic amorphous Fe nanoparticles embedded in SiO_2 glass matrices [36].

The main resonance signal is due to an FMR uniform mode which corresponds to a uniform precession of all the magnetic moments coupled to the Ni particles. In Figure 4, we see with increasing frequency the shift of the uniform mode to a higher field. The uniform mode frequency [34–38] may be obtained in the form $\omega_{\text{res}} = \gamma(H_{\text{res}} + H_{\text{int}})$, where γ is the effective gyromagnetic ratio, and H_{res} and H_{int} denote the resonance field at frequency, $\omega_{\text{res}}/2\pi$, and the internal field, respectively. The data in Figure 5 show how the resonance

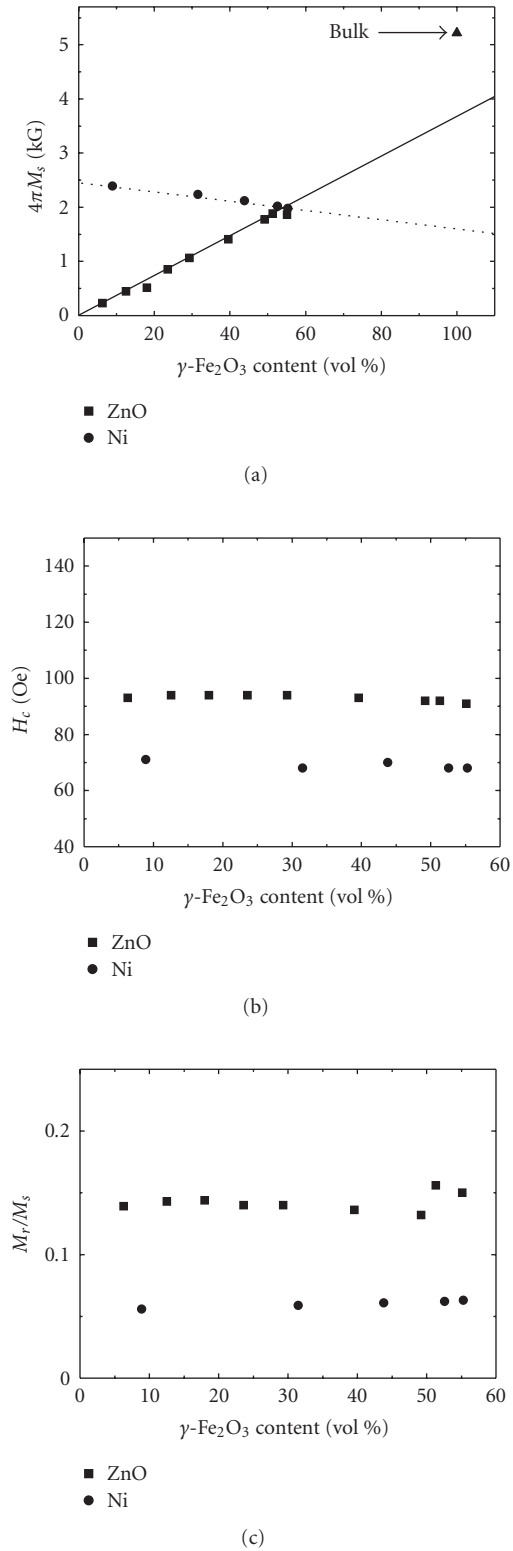

Figure 3: (a) Variation of the saturation magnetization $4\pi M_s$ as a function of γ-Fe_2O_3 content in Ni/γ-Fe_2O_3 and γ-Fe_2O_3/ZnO samples. The data for γ-Fe_2O_3/ZnO are from [21]. Room temperature. Squares (resp., triangles) denote γ-Fe_2O_3/ZnO (resp., Ni/γ-Fe_2O_3) NCs. The solid line shows an extrapolation of the linear $4\pi M_s$ response up to 100 vol % Ni. The dashed line is a guide for the eye; (b) Same as in (a) for the coercivity H_c; (c) Same as in (a) for the squareness M_r/M_s.

frequency evolves with H_{res}. From the slope of the linear functional $\omega_{\text{res}}(H_{\text{res}})$, we find that γ is in the range from 1.28 to 1.76 10^7 $\text{Oe}^{-1}\text{s}^{-1}$ (see Figure 6(a)). The offset of the frequency data versus magnetic field serves to obtain the internal field H_i. The difference between Ni/ZnO and Ni/γ-Fe_2O_3 NCs is most clearly seen in Figure 6(b). Here, H_i is shown as a function of Ni concentration. The main effect of increasing the Ni content is to increase significantly H_i for the Ni/ZnO NCs, for example, for Ni/ZnO H_i (40 vol %) exceeds by a factor of three the corresponding value for Ni/γ-Fe_2O_3. As mentioned earlier, (long-range) magnetostatic intergranular interactions dominate the exchange (short-range) in these NCs. This explains the changes in the effective field $H_{\text{eff}} = H_{\text{int}} + 4\pi M_s$ as the Ni content is increased (Figure 6(c)).

Additional insight into the relationship between composition, magnetic species, and resonance properties can be gained by comparing the FMR absorption versus field derivative profiles for Ni/ZnO (see Figure 4) and Ni/γ-Fe_2O_3 (see Figure 7) NCs. Overall, the profiles displayed in Figure 7 are more complicated than those discussed above. The derivative profiles for the main resonance are distorted by the presence of higher spin-wave modes for all sample and frequency investigated. One sees large departures from a Lorentzian-line shape which eventually indicates complicated interaggregates dipolar interactions, particularly in samples with large volume-filling factor. However, when one looks at the uniform mode frequency, plotted in Figure 8 as a function of the resonance field, one finds a much more linear increase than before. The values of γ associated with this plot change little and are in the range from 1.56 to 1.63 10^7 Oe^{-1} s^{-1} (see Figure 9(a)) to be compared with those previously determined in γ-Fe_2O_3/ZnO NCs which were in the range 1.70–1.82 10^7 Oe^{-1} s^{-1}. We can also compare the FMR absorption versus field derivative profiles for Ni/γ-Fe_2O_3 (see Figure 7) and γ-Fe_2O_3/ZnO (see [21, Figure 1]) NCs. Perhaps the most glaring difference with regard to γ-Fe_2O_3 concentration between Ni/γ-Fe_2O_3 and γ-Fe_2O_3/ZnO NCs is the influence of the internal field (see Figure 9(b)), constant and of the order of 500 Oe, on the significant increase of the effective field (Figure 9(c)) for γ-Fe_2O_3/ZnO samples while H_{eff} for the Ni/γ-Fe_2O_3 samples is a smoothly decreasing function of γ-Fe_2O_3 content. Therefore, magnetostatic interactions can be tuned by the choice of the magnetic species in these NCs.

The absorption profiles of loss versus field were obtained by integration of the raw data after baseline correction. An example (for a nominal frequency of 16 GHz) of FMR absorption curve of microwave loss versus static magnetic field is shown in Figure 10. The analysis of the FMR peak shapes cannot be realized by making the assumption that the resonance has a simple Lorentzian-line shape. However, we note that the FMR peak shape changes from a Lorentzian to a more complex shape for sufficiently large values of frequency. It is important to ask how well the simulations match the data based on least-square fitting using a pure Lorentzian profile. An example of this type of plot for an Ni/ZnO NC with 25.5 vol % is shown in the inset of Figure 10. Using this approach predicts linewidths that may be significantly different from measured values at low (<10 GHz) and high frequencies (>25 GHz). However, at intermediate frequencies,

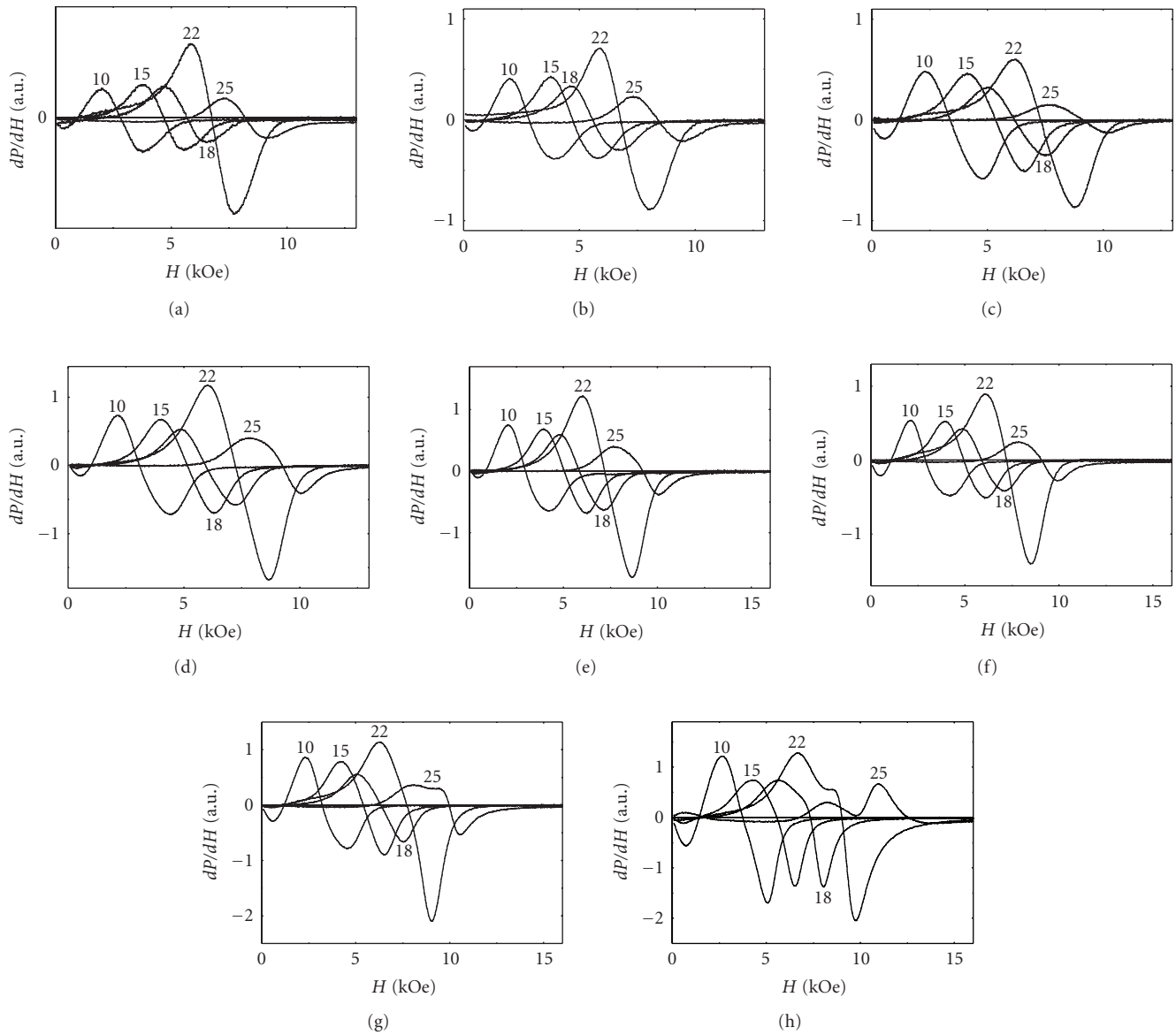

FIGURE 4: (a) Variation with magnetic field of the absorbed power derivative at different frequencies for the Ni/ZnO samples considered in the present study. Room temperature. The value of the frequency in GHz is indicated on each curve. nNIZ8 sample (Ni content is 8.9 vol %); (b) nNIZ7 sample (Ni content is 17.5 vol %); (c) nNIZ6 sample (Ni content is 25.5 vol %); (d) nNiZ5 sample (Ni content is 29.2 vol %); (e) nNiZ4 sample (Ni content is 33.4 vol %); (f) nNiZ3 sample (Ni content is 37.8 vol %); (g) nNiZ2 sample (Ni content is 41.8 vol %); (h) nNiZ1 sample (Ni content is 49.5 vol %).

for example, at a nominal frequency of 16 GHz, we find that the difference is at most ±3%. Although FMR data taken separately could often be treated in impressive detail a consistent overall model of microwave losses has not been reached. Thus, in the discussion to follow, the FMR absorption curve has been primarily modeled in terms of a Lorentzian-line shape (at 16 GHz) and we will advance only a qualitative analysis of the FMR response.

3.3. Discussion

The issues and results outlined in the previous subsections call for further comment on: (a) the interpretation of the peak-to-peak linewidth in terms of the Gilbert effective damping parameter α, and (b) the role of anisotropy.

Commencing with item (a), we note that one of the major challenges for describing the dynamic magnetic response of magnetic heterostructures is the characterization of the damping mechanisms. Many theoretical approaches have been applied. Smith [39] has shown how fluctuation-dissipation arguments can discriminate between alternative phenomenological damping models, for example, inhomogeneity and finite-size effects, which can complement traditional uniform magnetization descriptions of damped ferromagnetic resonance (FMR). A tensor of damping which reflects the anisotropy of the magnetic system was also derived

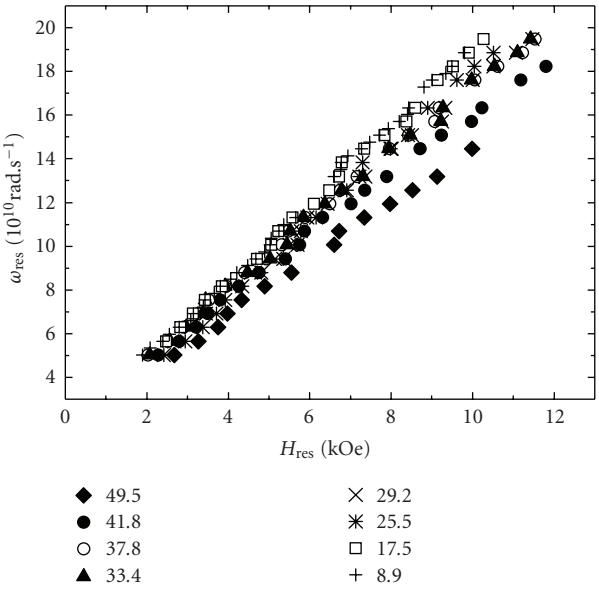

FIGURE 5: Dependence of the resonance frequency as a function of the resonance field. Room temperature. Symbols denote the volume fraction of Ni. The slope of the linear dependence is in the range 1.28 to 1.76 10^7 Oe^{-1} s^{-1} for all samples.

by Safonov et al. [40–44]. Unfortunately, the damping processes in these materials often possess a manifestly phenomenological nature, and so many ab initio approaches, including the deterministic Landau-Lifshitz equation of motion with the Gilbert form for the magnetic damping term $\partial_t \mathbf{M} = -\gamma \mathbf{M} \times \mathbf{H}_{\text{eff}} + (\alpha/M_s)\mathbf{M} \times \partial_t \mathbf{M}$, have significant difficulties with incorporating all damping mechanisms even for a monodomain ferromagnetic material, that is, beside intrinsic damping, there is also damping due to surface an interface effects, and interparticle interactions. In this continuum theory, $\mathbf{M}$ is the magnetization density, with magnitude $|\mathbf{M}| = M_s$ equal to the saturation magnetization, γ is the gyromagnetic ratio and is given by $\gamma = g\mu_B/\hbar$, where μ_B is the Bohr magneton moment and the Landé g factor (spectroscopic splitting factor), α is the dimensionless Gilbert-damping parameter [45–54]. $\mathbf{H}_{\text{eff}}$ is the local (effective) magnetic field acting on $\mathbf{M}$, which can include magnetostatic fields of external sources, crystal anisotropy, shape-dependent dipolar interactions, and exchange interactions which govern ferromagnetic spin-wave spectral characteristics [55].

We first turn our attention to the determination of the effective linewidth ΔH determined at 16 GHz. In Figure 11 (resp., Figure 12), we compare the Ni (resp., γ-Fe_2O_3) volume fraction dependence of ΔH for the series of samples considered here. The results in these figures are for 16 GHz. The interesting information contained in Figures 11 and 12 is that there is a clear difference in the variation of ΔH with composition. In Ni/ZnO and Ni/γ-Fe_2O_3 NCs, ΔH is in the range 1.8–2.6 kOe and increases linearly with Ni content. In Ni/γ-Fe_2O_3 and γ-Fe_2O_3/ZnO, ΔH was roughly on the same order, but with important differences in the rate of increase (resp., decrease) with γ-Fe_2O_3 content and the zero linewidth intercepts for γ-Fe_2O_3/ZnO (resp., Ni/γ-

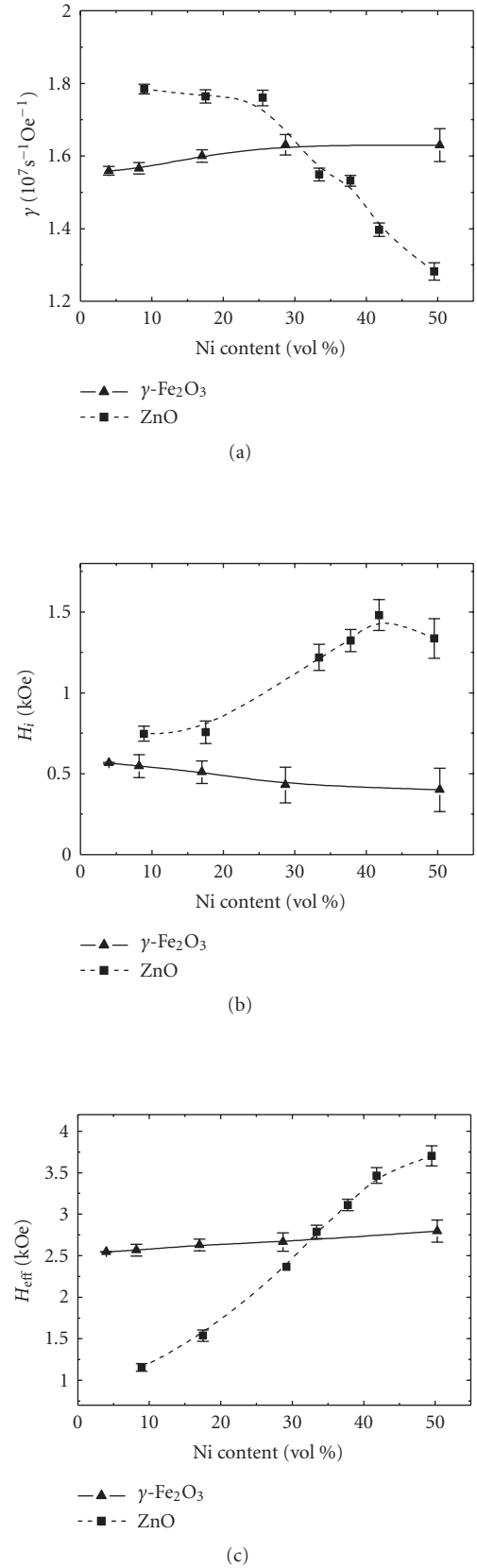

FIGURE 6: Comparison of the values of the gyromagnetic factor, γ, internal field, H_i, and, effective field, H_{eff}, for Ni/ZnO and Ni/γ-Fe_2O_3 samples as a function of the volume fraction of Ni. Room temperature. The solid and dashed lines serve to guide the eye.

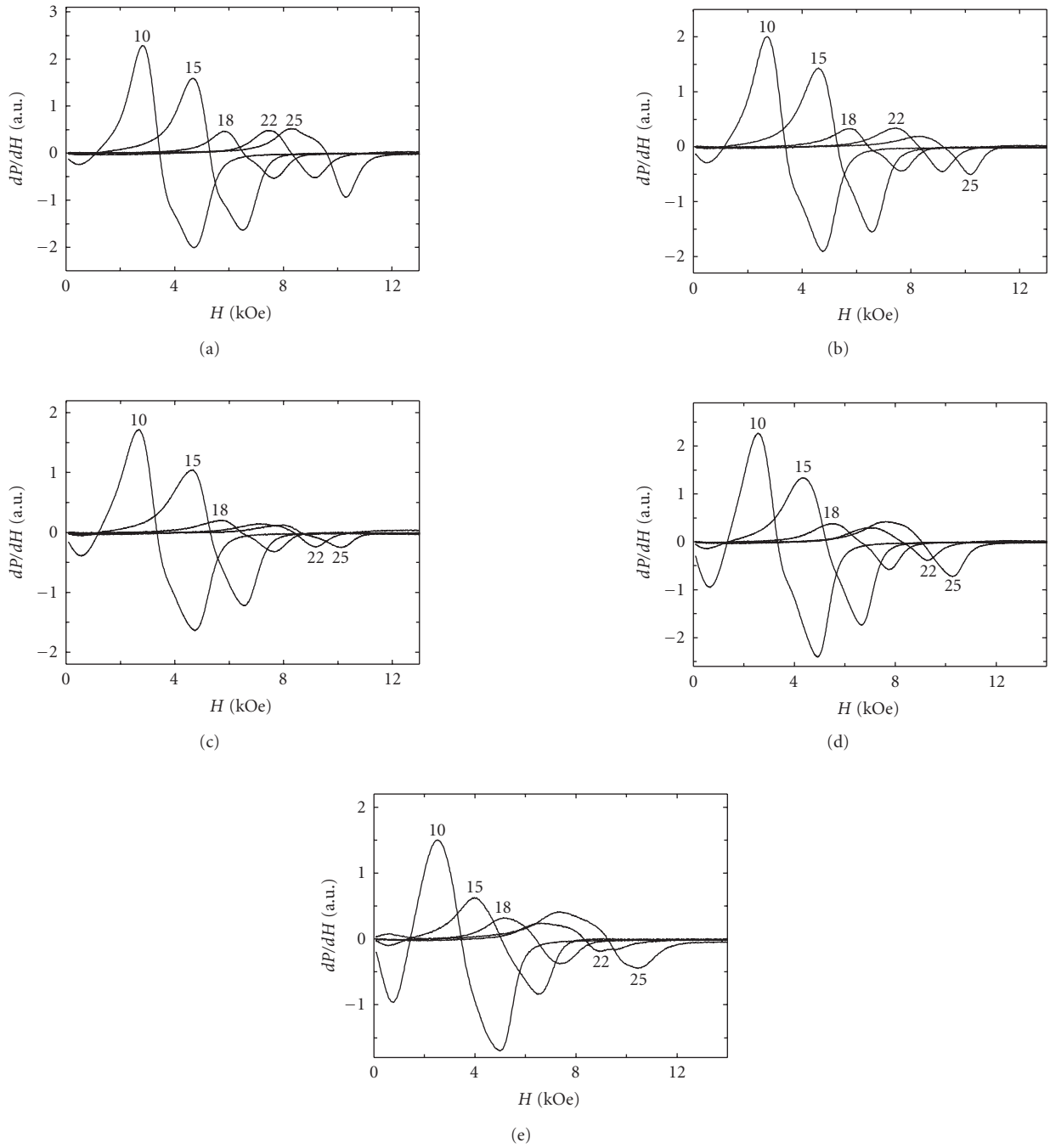

FIGURE 7: Same as in Figure 4 for Ni/γ-Fe_2O_3 samples considered in the present study. The value of the frequency in GHz is indicated on each curve. (a) 5-nNiF sample (4 vol % Ni and 55 vol %γ-Fe_2O_3); (b) 1-nNiF sample (8.2 vol % Ni and 53 vol %γ-Fe_2O_3); (c) 2-nNiF sample (17 vol % Ni and 44 vol %γ-Fe_2O_3); (d) 3-nNiF sample (28 vol % Ni and 32 vol %γ-Fe_2O_3); (e) 4-nNiF sample (50.3 vol % Ni and 9 vol %γ-Fe_2O_3). It is worth observing that the total magnetic volume fraction contained in these samples is nearly constant $\cong$ 60 vol %.

Fe_2O_3). The conductivity of a metal/insulator NC system can be dramatically decreased compared with conventional metallic alloys, leading to significantly reduced eddy current losses. It was emphasized by Ramprasad et al. [56] that eddy current losses of composites consisting of ferromagnetic (monodisperse) particles embedded in a nonmagnetic matrix are negligible below 10 GHz, if the particle radii are smaller than 100 nm, while composites with larger particles display significant effective permeability degradation. However, the effect of substitution of a magnetic phase (high conductivity) by a nonmagnetic phase (low conductivity) in the γ-Fe_2O_3 surrounding matrix is not related to the composition dependent conductivity [17]. Further work is needed to determine the origin of the FMR linewidth contributions displayed in Figure 12, but in any event the slopes of opposite sign indicate that they are clearly different for γ-Fe_2O_3/ZnO

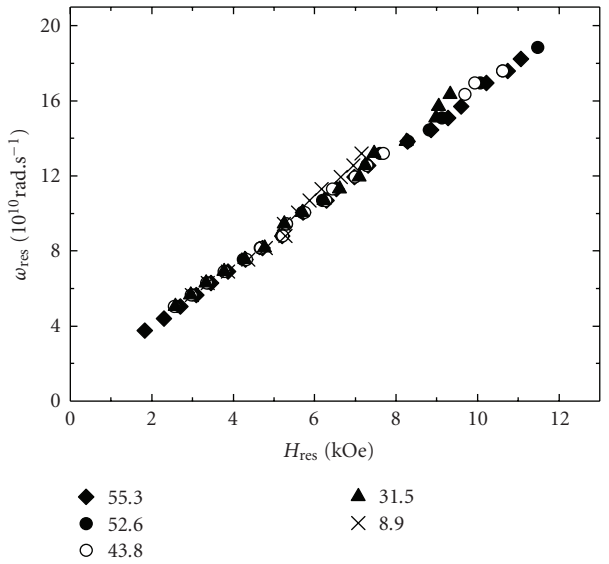

FIGURE 8: Same as in Figure 5 for Ni/γ-Fe_2O_3 samples considered in the present study. Symbols denote the volume fraction of Ni. The slope of the linear dependence is in the range 1.56 to 1.63 10^7 Oe^{-1} s^{-1} for all samples.

and Ni/γ-Fe_2O_3. The apparent match in $\Delta H \cong 2$ kOe when the two straight lines cross each other at approximately 50% vol may be fortuitous (see Figure 12).

The effective linewidth, defined as the full width at half maximum of the absorption curve, is an important feature of the FMR modes. There are two main contributions to the linewidth: intrinsic and extrinsic. The intrinsic contribution is due to damping and is a fundamental characteristic of the magnetic material. The extrinsic contribution is due to the magnetic inhomogeneities which are contained into the material and anisotropy dispersion within the material. The peak-to-peak FMR linewidth of the uniform resonance mode ΔH gs related to the damping parameter α and is given by $\Delta H = 2\alpha\omega/\sqrt{3}\gamma$, where ω is the angular frequency of the exciting field and where the coefficient of $1/\sqrt{3}$ is the correction of the difference between the full width at half maximum and the peak-to-peak linewidth for the Lorentzian-line shape. The observed effective ΔH and α are believed to be the result of inhomogeneity-related relaxation processes which increase the FMR linewidth from intrinsic values. Overall, one can say that the value effective damping parameter which is in the range 0.21–0.37 (see the inset of Figures 11 and 12) is consistent with the fact that for nanoparticles the damping parameter can exceed the bulk value for one order of magnitude or more [55–57].

As noted in Section 1, another perspective to characterize these NCs came from the study of microwave properties using spin-wave (SW) spectroscopy [23]. The relative change of SW group velocity induced by the samples was observed to depend significantly on the chemical composition and volume fraction of magnetic species contained in the NC. It was argued that the peaks in the losses have a magnetic character and are due to spin excitations of magnetic nanoparticles. It was also observed that the variation of the SW velocity in

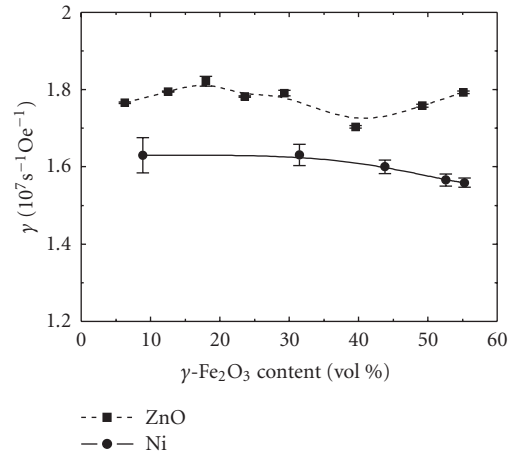

(a)

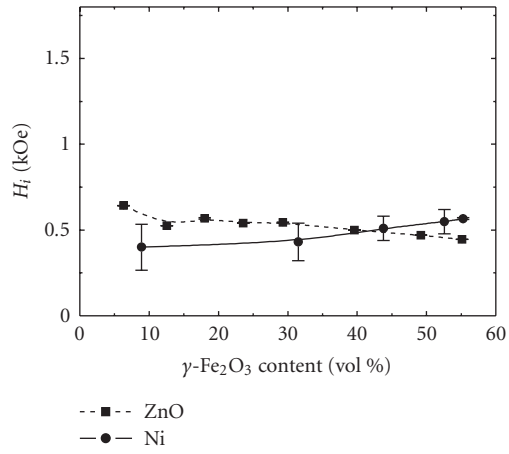

(b)

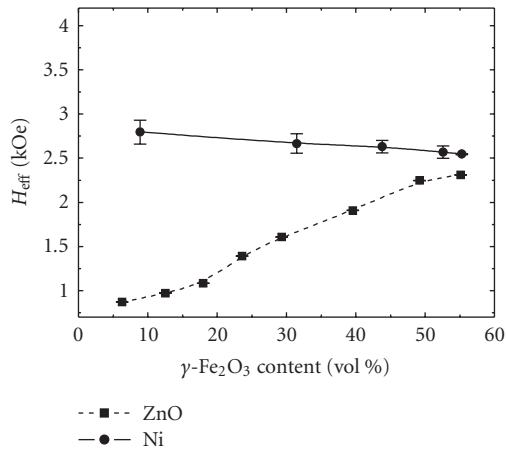

(c)

FIGURE 9: Same as in Figure 6 for Ni/γ-Fe_2O_3 and γ-Fe_2O_3/ZnO samples as a function of the volume fraction of γ-Fe_2O_3. The solid and dashed lines serve to guide the eye.

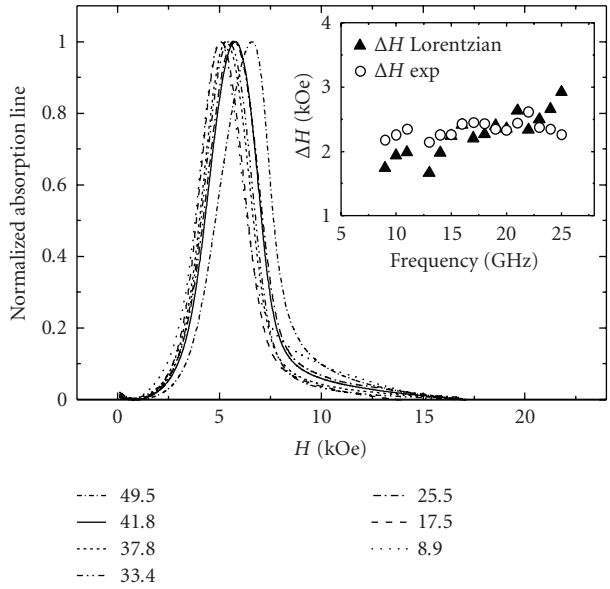

Figure 10: Integrated profiles for the derivative FMR profiles versus the static external magnetic field at 16 GHz for the Ni/ZnO samples considered in the present study. Room temperature. The value of the Ni content in vol % is indicated on each curve. The inset compares the peak-to-peak FMR effective linewidth obtained from the measurements (∘) and that derived by assuming a pure Lorentzian profile (▲).

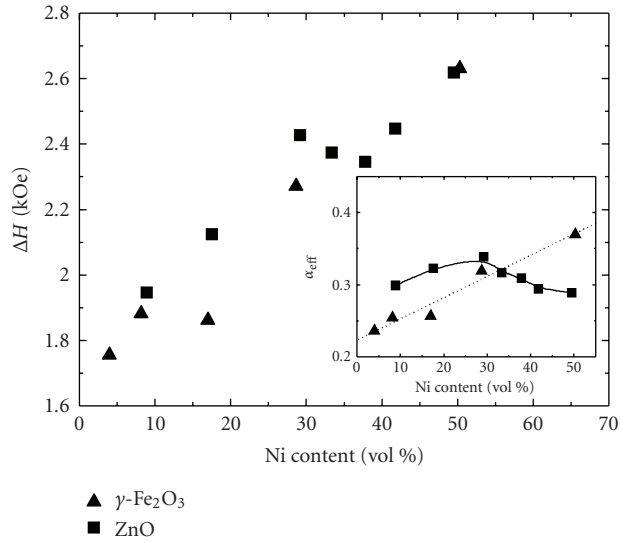

Figure 11: The peak-to-peak resonance effective linewidth as a function of Ni content for Ni/ZnO and Ni/γ-Fe_2O_3 samples. The inset shows the variation of the effective Gilbert damping parameter determined for a nominal frequency of 16 GHz for Ni/γ-Fe_2O_3 and Ni/ZnO samples as a function of Ni content. The solid and dashed lines serve to guide the eye.

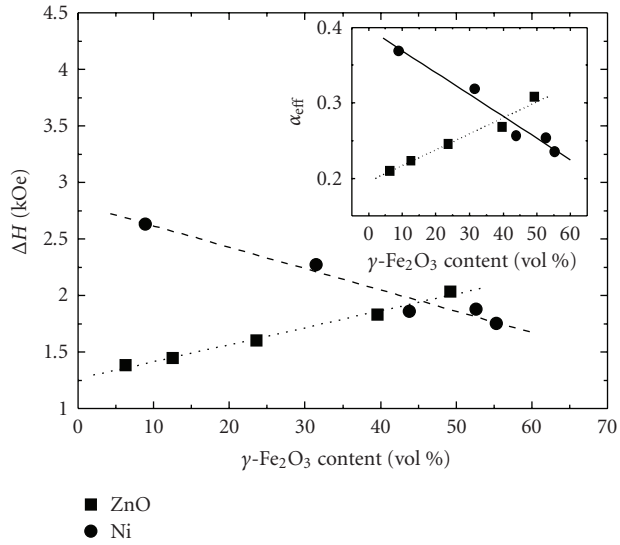

Figure 12: Same as in Figure 11 for Ni/γ-Fe_2O_3 and γ-Fe_2O_3/ZnO samples as a function of γ-Fe_2O_3 content.

Ni/ZnO and Ni/γ-Fe_2O_3 showed opposite trends when the data were plotted as a function of Ni concentration.

Now concerning item (b), we make several observations related to the surface anisotropy contribution to the anisotropy of Ni and γ-Fe_2O_3 nanoparticles. Surface anisotropy becomes important only for particles with size less than, say, 100 nm. In this sub-100-nm regime, magnetic particles are single domain but the particles eventually form aggregates and apart from the dipolar interaction between the nanoparticles, other types of interactions, for example, intracluster exchange, may also become relevant. The magnetic properties of nanophases are determined both by the behavior of particles and by the spatial distribution of the aggregates which defines the magnetostatic interactions between them. As we have noticed earlier, the distance of closest approach between particles is expected to be large enough for the interactions to have mainly a magnetostatic character. It is interesting to observe that a set of bounds for the effective permeability of composites containing spherical (monodisperse) particles with a ligand shell coating was derived by Ramprasad et al. [56], showing that this physicochemical attribute of the particles may become relevant when the ligand shell thickness is large compared to the particle radius. As previously mentioned [22], it is believed that the differences observed in the gyromagnetic resonance spectra observed between the NCs are a consequence of effective magnetic anisotropy.

We would like to emphasize that the exact oxidation state and oxidation-layer thickness of Ni nanoparticles in the NCs are unknown. Because the samples have been prepared in ambient atmosphere, surface passivation by a thin layer of nickel oxide NiO is inevitable. Due to the large surface-area-to-volume ratio, oxidation seems to be a persistent problem in core-shell nanoparticles. There have been a number of contributions to this problem, and although there is a consensus that the oxidation state of Ni has an impact on the magnetic properties, there is still ongoing debate on the role of oxide, with recent evidence from ^{57}Fe Mössbauer

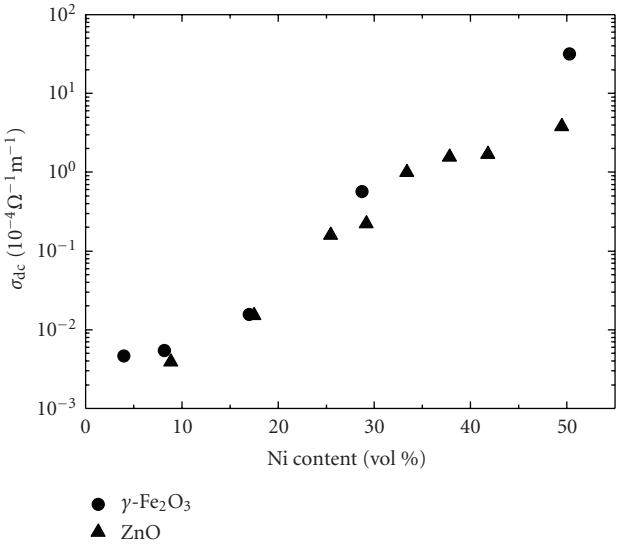

Figure 13: Experimental values of the dc conductivity of Ni/ZnO (▲) and Ni/γ-Fe_2O_3 (•) NCs, measured by the four-point probe technique, as a function of Ni content. Room temperature.

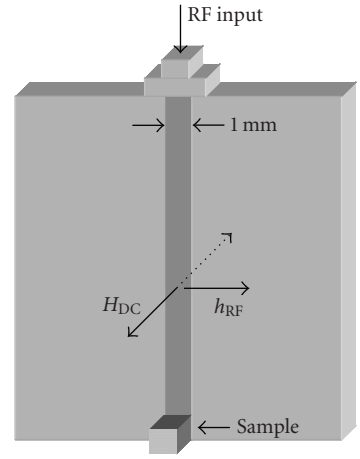

Figure 14: Schematic description of the microstrip line employed for the FMR measurements (in-plane field geometry). The transmission stripline (Au) of 1 mm width and a length of 10 mm is designed to have 50 Ω impedance above 4 GHz. It was fabricated by UV lithography and deposited on a 5 mm thick alumina substrate with a bottom conducting ground plane.

spectroscopy, neutron powder diffraction and magnetization studies of the properties of mixtures of (ferromagnetic) γ-Fe_2O_3 and (antiferromagnetic) NiO nanoparticles, indicating that the mixing of γ-Fe_2O_3 nanoparticles with NiO nanoparticles results in a faster superparamagnetic relaxation and a reduced coercivity compared to a sample consisting solely of γ-Fe_2O_3 nanoparticles [57]. This point may also underline the propensity of the material or defects within the NC to provide oxidation sources for the metal nanocrystals since it influences greatly the microwave magnetic response. We further note that the development of magnetic metal nanoparticles has been limited by the fact that they oxidize in air, forming either weakly magnetic or nonmagnetic oxides, resulting in the generation of stresses [58, 59].

4. CONCLUDING REMARKS

We have presented a detailed study on the magnetization and FMR response of Ni/ZnO and Ni/γ-Fe_2O_3 NCs. To summarize, the immediate conclusions that we can make from the experimental results presented above are as follows: (i) the analysis of the FMR spectra can be interpreted as arising from aggregates of magnetic nanoparticles, each of which resonates in an effective magnetic field composed of the applied field, the average (magnetostatic) dipolar field, and the randomly oriented magnetic anisotropy field; (ii) referring to the experimental data, it has been established that inhomogeneity-based line-broadening mechanisms, due to the damping of surface/interface effects and interparticle interaction, affect the FMR effective linewidth. The large value of the peak-to-peak linewidth cannot be taken as a representation of the intrinsic losses due to the inhomogeneous line-broadening contribution; (iii) particularly important is the fact that the FMR peak shape changes from a Lorentzian to a more complex shape showing distorsions for sufficiently

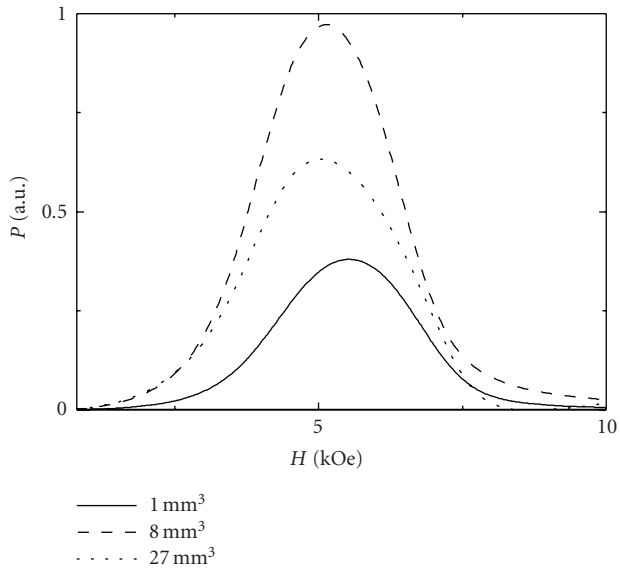

Figure 15: Ferromagnetic resonance profiles at 16 GHz. The graphs show the absorbed power versus applied magnetic field for a representative Ni/ZnO cubic shape sample (nNiZ6 containing 25 vol % Ni and 35 vol % ZnO) for three volumes: 1, 8, and 27 mm^3, as indicated. Room temperature.

large values of frequency. Details of the origins of these distorsions are not entirely clear; (iv) a comparison between the linewidth for granular metal and metal oxide NCs proves interesting in the FMR experiments.

It has been widely recognized that, at all length scales, the scale-relative properties of electromagnetic and magnetic systems vary with their size due to increasing edge-to-surface and surface-to-volume ratios. Thus, engineering useful NCs

will require an understanding of how the physical properties of aggregates evolve with size and shape into those of bulk NCs. As recalled earlier, an additional problem is particle oxidation arising from the large surface-area-to-volume ratio. The fundamental nature of oxidation in nanometer-sized structures has received some recent attention [60–64], however it is far from being well understood.

Before we conclude, we place our results in perspective. Challenges towards multiple functionality in NCs include design and preparation of materials that exhibit electric and magnetic fields-tunable electromagnetic wave transport properties. We are currently engaged in a systematic investigation of loss minimization of NCs for optimizing microwave applications. In a broader context, a similar analysis is planned for a series of piezoelectric-magnetostrictive NCs with a systematic variation in composition, control of internal strain, and magnetoelastically induced anisotropy due to large stress between the nanoparticles and the surrounding matrix, impurities, and porosity since it is well established that all of these preparation parameters are known to produce large linewidths. For that purpose, the consolidation of high density NCs, that is, by using hot pressing [65], or hot isostatic pressing [66, 67], is a critical step towards development of an optimal soft magnetic NC.

APPENDICES

A. EVALUATION OF CONDUCTIVITY AND SKIN EFFECT AND EDDY CURRENT ANALYSIS

In this appendix, we describe several details of the measurement of the dc conductivity, σ_{dc}, of our NCs using the four-point probe technique. In Figure 13, we show $\sigma_{dc}(f_{Ni})$ for Ni/ZnO samples. From Figure 13, we observe that the data collected at low field exhibit an exponential increase between 10 and 40 vol % Ni and a change of slope at about 40 vol % Ni. In electrodynamics [68, 69], it has been traditional to consider the skin depth as the distance δ through which the amplitude of the propagating wave decreases by a factor e^{-1}. For our low-conductivity NCs and considering the measured values of the effective electromagnetic parameters of these NCs [17, 18], we find that δ is in the 10^2–10^3 mm size range in the GHz frequency range, that is, much larger than the sample thickness. Thus, one can safely assume a full penetration of the microwave field into our samples. Similar measurements for the Ni/γ-Fe_2O_3 NCs indicate that the values of $\sigma_{dc}(f_{Ni})$ are close to the values for Ni/ZnO NCs. Another important issue which has been previously discussed in [17] is the possibility of a direct observation of the intrinsic complex permittivity of the magnetic phases based on the measurement of the effective complex permittivity of the NCs and using a mean-field (effective medium) theory, for example, Bruggeman, McLachlan. At present there is no universal agreement about an effective medium theory that can self-consistently explain the various experimental measurements probing the dielectric properties of NC. We refer the interested reader to [17] for the details of the derivation. No conduction (percolation) threshold is evidenced indicating a disconnected nanoparticles network. In these powder compact composites, the presence of insulating grains and of the amorphous epoxy resin increases the conduction barrier height and therefore is expected to decrease the overall conductivity of the samples. However, even if the volume fraction of the nanoparticles—and hence the intergrain spacing—and grain size were independently adjustable, we have not yet studied the local charge transport mechanisms.

Several comments are in order. First, in composite with uniform dispersions of magnetic nanoparticles, the conductivity of the NC is determined mainly by the interparticle distance and eddy currents, produced within the particle that are extremely small at high frequency, are limited to individual particles or aggregates. We note that Ramprasad et al. [56] have shown, in their phenomenological modeling of the properties of magnetic nanoparticle composites, that in the 0.1–10 GHZ frequency range, particles with radii smaller than 100 nm are expected to encounter negligible eddy current losses. This was found true even at high particle volume fraction, when clustering of particles could result in aggregates much larger than the actual particles. Second, no signature for percolation threshold is apparent for the data collected; thus we infer from the weak f_{Ni} dependence of σ_{dc} that the Ni nanoaggregates should be separated in the ZnO matrix. It is well established by now that in ferromagnetic NCs, the shielding and dissipation due to eddy currents rapidly diminish with decreasing the particle size [70]. This has for effect to reduce the dielectric losses in metallic nanoparticles. Third, with dimensions of NCs well below the skin depth, the electromagnetic wave fully penetrates the sample and allows the contribution of the whole volume to the magnetic properties of the NCs.

B. INFLUENCE OF SAMPLE SHAPE ON INHOMOGENEOUS BROADENING

The purpose of this appendix is to briefly discuss the issue raised in Section 2.1, namely, the choice of the dimensions of our NC samples. Cubes with different nominal thickness in the millimeter size range were fabricated. The specific data shown in the experimental section (Figures 4 and 7) are for a 1 mm thick cube. Intuitively, one expects the present experimental condition to apply for sample thickness comparable or smaller than the width (1 mm) of the microstrip line (with reference to Figure 14). The samples were placed in the microstrip with the homogeneous external static magnetic field applied perpendicular to the sample and the linearly polarized microwave excitation field h_{rf} in the sample plane.

Strictly speaking, the FMR equation that was used to determine the FMR field is only valid for spherical samples [37]. It has been widely recognized that because of inhomogeneities in the demagnetization field this may affect the broadening of the FMR peak. To discriminate between sample thickness and material on the observed broadening, we varied the thickness of our cubic samples. We illustrate the influence of the sample thickness (see Figure 14) for the absorbed power change of a representative sample (nNiZ6 containing 25 vol % Ni) as a function of applied magnetic field. These absorption profiles of loss versus field were obtained

from direct integration of the raw data (measured derivative of the absorbed power versus applied magnetic field). One can see that the peak loss points in the graphs in Figure 15 are shifted up in field for the two smaller samples. The effective linewidth, taken as the full width at half maximum of the profiles in Figure 15, are 2.4 kOe (resp., 2.5 kOe and 3.1 kOe) for the 1 (resp., 2 and 3) mm thick sample. The asymmetry of the absorption profile apparent for the $2 \times 2 \times 2$ and $3 \times 3 \times 3\,\text{mm}^3$ samples is indicative of a departure from a Lorentzian line. Such inhomogeneously broadened line originates from a complicated interaggregate dipolar interaction due to large residual strains and porosity. On the other hand, the line shape for the 1 mm thick sample is symmetric. Increasing the thickness by a factor of three does not strongly change the FMR linewidth of the integrated power of the uniform mode itself, and indicates that H_{res} (at 16 GHz) is not appreciably affected. The fact that no increase in FMR linewidth with thickness is evidenced supports also the conclusion that eddy current losses are negligible for this sample.

This interpretation also resonates well with the recent FMR and high-frequency analysis of ferrite-ferroelectric composite materials by Kalarickal et al. [35], who studied how the shape (cubes and spheres with nominal diameters of 2 mm) of their composite samples influences the static magnetic properties. They found that cubes and spheres gave similar results for all the effective loadings of the ferrite component. Their FMR measurements were made on nominal 1 mm diameter spheres (for 100% ferrite material) or 3 mm diameter spheres (for the materials with lower loadings). Guskos et al. [71] investigated by FMR polymer composites containing as filler a binary mixture of Fe_3O_4 and FE_3C nanoparticles (30–50 nm) dispersed in a diamagnetic carbon matrix. These authors placed a square-shaped sample of $3.5 \times 3.5\,\text{mm}^2$ cut out from the polymer sheet in the center of a TE_{102} cavity, that is, at the local maximum of the microwave magnetic component and in the nodal plane of the electric component.

ACKNOWLEDGMENT

The first author acknowledges the financial support from the Conseil Régional de Bretagne for a Ph.D. studentship.

REFERENCES

[1] S. A. Wolf, D. D. Awschalom, R. A. Buhrman, et al., "Spintronics: a spin-based electronics vision for the future," *Science*, vol. 294, no. 5546, pp. 1488–1495, 2001.

[2] M. Fiebig, "Revival of the magnetoelectric effect," *Journal of Physics D*, vol. 38, no. 8, pp. R123–R152, 2005.

[3] V. Skumryev, S. Stoyanov, Y. Zhang, G. Hadjipanayis, D. Givord, and J. Nogués, "Beating the superparamagnetic limit with exchange bias," *Nature*, vol. 423, no. 6942, pp. 850–853, 2003.

[4] R. F. Ziolo, E. P. Giannelis, B. A. Weinstein, et al., "Matrix-mediated synthesis of nanocrystalline γ-Fe_2O_3: a new optically transparent magnetic material," *Science*, vol. 257, no. 5067, pp. 219–223, 1992.

[5] A. F. Bakuzis, K. S. Neto, P. P. Gravina, et al., "Magneto-optical properties of a highly transparent cadmium ferrite-based magnetic fluid," *Applied Physics Letters*, vol. 84, no. 13, pp. 2355–2357, 2004.

[6] H. S. Nalwa, Ed., *Encyclopedia of Nanoscience and Nanotechnology*, American Scientific, New York, NY, USA, 2004.

[7] E. L. Wolf, *Nanophysics and Nanotechnology*, Wiley-VCH, Weinheim, Germany, 2004.

[8] G. Cao, *Nanostructures and Nanomaterials*, Imperial College Press, London, UK, 2004.

[9] H. Schmid, "Magnetoelectric effects in insulating magnetic materials," in *Introduction to Complex Mediums for Optics and Electromagnetics*, W. S. Wieglhofer and A. Lakhtakia, Eds., pp. 167–195, SPIE Press, Bellingham, Wash, USA, 2003.

[10] J. Wang, J. B. Neaton, H. Zheng, et al., "Epitaxial $BiFeO_3$ multiferroic thin film heterostructures," *Science*, vol. 299, no. 5613, pp. 1719–1722, 2003.

[11] J. Baker-Jarvis and P. Kabos, "Dynamic constitutive relations for polarization and magnetization," *Physical Review E*, vol. 64, no. 5, Article ID 056127, 14 pages, 2001.

[12] J. Zhai, J. Li, D. Viehland, and M. I. Bichurin, "Large magnetoelectric susceptibility: the fundamental property of piezoelectric and magnetostrictive laminated composites," *Journal of Applied Physics*, vol. 101, no. 1, Article ID 014102, 4 pages, 2007.

[13] R. S. Devan and B. K. Chougule, "Effect of composition on coupled electric, magnetic, and dielectric properties of two phase particulate magnetoelectric composite," *Journal of Applied Physics*, vol. 101, no. 1, Article ID 014109, 6 pages, 2007.

[14] G. B. Smith, "Nanostructured thin films," in *Introduction to Complex Mediums for Optics and Electromagnetics*, W. S. Wieglhofer and A. Lakhtakia, Eds., SPIE Press, Bellingham, Wash, USA, 2003.

[15] V. Kochergin, V. Zaporojtchenko, H. Takele, F. Faupel, and H. Föll, "Improved effective medium approach: application to metal nanocomposites," *Journal of Applied Physics*, vol. 101, no. 2, Article ID 024302, 7 pages, 2007.

[16] C. Brosseau, J. Ben Youssef, P. Talbot, and A.-M. Konn, "Electromagnetic and magnetic properties of multicomponent metal oxides heterostructures: nanometer versus micrometer-sized particles," *Journal of Applied Physics*, vol. 93, no. 11, pp. 9243–9256, 2003.

[17] C. Brosseau and P. Talbot, "Effective permittivity of nanocomposite powder compacts," *IEEE Transactions on Dielectrics and Electrical Insulation*, vol. 11, no. 5, pp. 819–832, 2004.

[18] C. Brosseau and P. Talbot, "Effective magnetic permeability of Ni and Co micro- and nanoparticles embedded in a ZnO matrix," *Journal of Applied Physics*, vol. 97, no. 10, Article ID 104325, 11 pages, 2005.

[19] S. Mallégol, C. Brosseau, P. Quéffelec, and A.-M. Konn, "Measurement of the permeability tensor in nanophases of granular metal oxides and field-induced magnetic anisotropy," *Physical Review B*, vol. 68, no. 17, Article ID 174422, 6 pages, 2003.

[20] C. Brosseau, S. Mallégol, P. Quéffelec, and J. Ben Youssef, "Nonreciprocal electromagnetic properties of nanocomposites at microwave frequencies," *Physical Review B*, vol. 70, no. 9, Article ID 092401, 4 pages, 2004.

[21] J. Ben Youssef and C. Brosseau, "Magnetization damping in two-component metal oxide micropowder and nanopowder compacts by broadband ferromagnetic resonance measurements," *Physical Review B*, vol. 74, no. 21, Article ID 214413, 13 pages, 2006.

[22] C. Brosseau, S. Mallégol, P. Quéffélec, and J. Ben Youssef, "Electromagnetism and magnetization in granular two-phase nanocomposites: a comparative microwave study," *Journal of Applied Physics*, vol. 101, no. 3, Article ID 034301, 15 pages, 2007.

[23] L. Lutsev, S. Yakovlev, and C. Brosseau, "Spin wave spectroscopy and microwave losses in granular two-phase magnetic nanocomposites," *Journal of Applied Physics*, vol. 101, no. 3, Article ID 034320, 8 pages, 2007.

[24] Y. Wu, J. Li, Z.-Q. Zhang, and C. T. Chan, "Effective medium theory for magnetodielectric composites: beyond the long-wavelength limit," *Physical Review B*, vol. 74, no. 8, Article ID 085111, 9 pages, 2006.

[25] S. A. Majetich and M. Sachan, "Magnetostatic interactions in magnetic nanoparticle assemblies: energy, time and length scales," *Journal of Physics D*, vol. 39, no. 21, pp. R407–R422, 2006.

[26] J. A. A. J. Perenboom, P. Wyder, and F. Meier, "Electronic properties of small metallic particles," *Physics Reports*, vol. 78, no. 2, pp. 173–292, 1981.

[27] M. Wu, Y. D. Zhang, S. Hui, et al., "Microwave magnetic properties of $Co_{50}/(SiO)_{50}$ nanoparticles," *Applied Physics Letters*, vol. 80, no. 23, pp. 4404–4406, 2002.

[28] K. Yamaura, D. P. Young, and R. J. Cava, "Thermally induced variable-range-hopping crossover and ferromagnetism in the layered cobalt oxide $Sr_2Y_{0.5}Ca_{0.5}Co_2O_7$," *Physical Review B*, vol. 63, no. 6, Article ID 064401, 5 Pages, 2001.

[29] A. R. Pereira, K. L. C. Miranda, P. P. C. Sartoratto, P. C. Morais, and A. F. Bakuzis, "Ferromagnetic resonance investigation of maghemite-silica nanocomposites," *Journal of Applied Physics*, vol. 100, no. 8, Article ID 086110, 3 Pages, 2006.

[30] H. M. Sauer, E. Cura, S. Spiekermann, and R. Hempelmann, "Nanoscaled nickel-zinc-iron oxides of spinell type as soft magnetic colloids and their ferromagnetic resonance spectrum," *Zeitschrift für Physikalische Chemie*, vol. 220, no. 2, pp. 189–198, 2006.

[31] W. Wong, H. Li, Z. R. Zhao, and J. C. Chen, "Magnetic coercivity of Fe_3O_4 particle systems," *Journal of Applied Physics*, vol. 69, no. 8, pp. 5119–5121, 1991.

[32] E. Tronc, D. Fiorani, M. Noguès, et al., "Surface effects in non-interacting and interacting γ-Fe_2O_3 nanoparticles," *Journal of Magnetism and Magnetic Materials*, vol. 262, no. 1, pp. 6–14, 2003.

[33] A. E. Berkowitz, W. J. Schuele, and P. J. Flanders, "Influence of crystallite size on the magnetic properties of acicular γ-Fe_2O_3 articles," *Journal of Applied Physics*, vol. 39, no. 2, pp. 1261–1263, 1968.

[34] M. Pardavi-Horvath and L. J. Swartzendruber, "Ferromagnetic resonance relaxation in reaction milled and annealed fe-zn nanocomposites," *IEEE Transactions on Magnetics*, vol. 35, no. 5, pp. 3502–3504, 1999.

[35] S. S. Kalarickal, D. Ménard, J. Das, et al., "Static and high frequency magnetic and dielectric properties of ferrite-ferroelectric composite materials," *Journal of Applied Physics*, vol. 100, no. 8, Article ID 084905, 9 pages, 2006.

[36] S. Tomita, M. Hagiwara, T. Kashiwagi, et al., "Ferromagnetic resonance study of diluted Fe nanogranular films," *Journal of Applied Physics*, vol. 95, no. 12, pp. 8194–8198, 2004.

[37] M. Sparks, *Ferromagnetic Relaxation Theory*, McGraw-Hill, New York, NY, USA, 1964.

[38] A. F. Kip and R. D. Arnold, "Ferromagnetic resonance at microwave frequencies in an iron single crystal," *Physical Review*, vol. 75, no. 10, pp. 1556–1560, 1949.

[39] N. Smith, "Fluctuation-dissipation considerations for phenomenological damping models for ferromagnetic thin films," *Journal of Applied Physics*, vol. 92, no. 7, p. 3877, 2002.

[40] V. L. Safonov, "Micromagnetic grain as a nonlinear oscillator," *Journal of Magnetism and Magnetic Materials*, vol. 195, no. 2, pp. 523–529, 1999.

[41] V. L. Safonov, "Thermal reversal of magnetization as "random walk" dynamics of a nonlinear oscillator," *Journal of Applied Physics*, vol. 85, no. 8, pp. 4370–4372, 1999.

[42] V. L. Safonov and H. N. Bertram, ""Dynamic-thermal" reversal in a fine micromagnetic grain: time dependence of coercivity," *Journal of Applied Physics*, vol. 87, no. 9, pp. 5681–5683, 2000.

[43] V. L. Safonov and H. N. Bertram, "Magnetization dynamics and thermal fluctuations in fine grains and films," in *The Physics of Ultra-high-Density Magnetic Recording*, M. Plumer, J. van Ek, and D. Weller, Eds., p. 81, Springer, Berlin, Germany, 2001.

[44] V. L. Safonov and H. N. Bertram, "Fluctuation-dissipation considerations and damping models for ferromagnetic materials," *Physical Review B*, vol. 71, Article ID 224402, 5 pages, 2005.

[45] A. Aharony, *Introduction to the Theory of Ferromagnetism*, Oxford University Press, New York, NY, USA, 1996.

[46] E. C. Stoner and E. P. Wohlfarth, "A mechanism of magnetic hysteresis in heterogeneous alloys," *Philosophical Transactions of the Royal Society of London*, vol. 240, pp. 599–642, 1948.

[47] A. H. Morrish, *The Physical Principles of Magnetism*, John Wiley & Sons, New York, NY, USA, 1965.

[48] T. L. Gilbert, "A Lagrangian formulation of the gyromagnetic equation of the magnetic field," *Physical Review*, vol. 100, p. 1243, 1955.

[49] L. Landau and E. Lifshitz, "On the theory of the dispersion of magnetic permeability in ferromagnetic bodies," *Physikalische Zeitschrift der Sowjetunion*, vol. 8, pp. 153–169, 1935.

[50] L. D. Landau, E. M. Lifshitz, and L. P. Pitaevski, *Statistical Physics*, Pergamon Press, Oxford, UK, 3rd edition, 1980.

[51] L. D. Landau, "On the theory of phase transition," in *Collected Papers of L. D. Landau*, D. ter Haar, Ed., p. 193, Gordon and Breach, New York, NY, USA, 1967.

[52] R. Kikuchi, "On the minimum of magnetization reversal time," *Journal of Applied Physics*, vol. 27, no. 11, pp. 1352–1357, 1956.

[53] W. F. Brown Jr., *Micromagnetics*, Wiley-Interscience, New York, NY, USA, 1963.

[54] H. Kronmüller and M. Fähnle, *Micromagnetism and the Microstructure of Ferromagnetic Solids*, Cambridge University Press, Cambridge, UK, 2003.

[55] W. F. Brown Jr., *Magnetostatic Principles in Ferromagnetism*, North-Holland, Amsterdam, The Netherlands, 1962.

[56] R. Ramprasad, P. Zurcher, M. Petras, M. Miller, and P. Renaud, "Magnetic properties of metallic ferromagnetic nanoparticle composites," *Journal of Applied Physics*, vol. 96, no. 1, pp. 519–529, 2004.

[57] C. Frandsen, C. W. Ostenfeld, M. Xu, et al., "Interparticle interactions in composites of nanoparticles of ferrimagnetic γ-Fe_2O_3 and antiferromagnetic (CoO,NiO) materials," *Physical Review B*, vol. 70, no. 13, Article ID 134416, 7 pages, 2004.

[58] H. S. Nalwa, Ed., *Encyclopedia of Nanoscience and Nanotechnology*, American Scientific, New York, NY, USA, 2004.

[59] H. E. Evans, "Stress effects in high temperature oxidation of metals," *International Materials Reviews*, vol. 40, no. 1, pp. 1–40, 1995.

[60] S.-J. Cho, J.-C. Idrobo, J. Olamit, K. Liu, N. D. Browning, and S. M. Kauzlarich, "Growth mechanisms and oxidation resistance of gold-coated iron nanoparticles," *Chemistry of Materials*, vol. 17, no. 12, pp. 3181–3186, 2005.

[61] K. S. Buchanan, A. Krichevsky, M. R. Freeman, and A. Meldrum, "Magnetization dynamics of interacting iron nanocrystals in SiO_2," *Physical Review B*, vol. 70, no. 17, Article ID 174436, 10 pages, 2004.

[62] C. A. Ross, "Patterned magnetic recording media," *Annual Review of Materials Science*, vol. 31, pp. 203–235, 2001.

[63] S. Sun and H. Zeng, "Size-controlled synthesis of magnetite nanoparticles," *Journal of the American Chemical Society*, vol. 124, no. 28, pp. 8204–8205, 2002.

[64] B. Ravel, E. E. Carpenter, and V. G. Harris, "Oxidation of iron in iron/gold core/shell nanoparticles," *Journal of Applied Physics*, vol. 91, no. 10, pp. 8195–8197, 2002.

[65] C. E. Patton, "Effect of grain size on the microwave properties of polycrystalline yttrium iron garnet," *Journal of Applied Physics*, vol. 41, no. 4, pp. 1637–1641, 1970.

[66] H. V. Atkinson and B. A. Rickinson, *Hot Isostatic Processing*, Adam Hilger, Bristol, UK, 1991.

[67] H. V. Atkinson and S. Davies, "Fundamental aspects of hot isostatic pressing: an overview," *Metallurgical and Materials Transactions A*, vol. 31, no. 12, pp. 2981–3000, 2000.

[68] L. Landau, E. M. Lifshitz, and L. P. Pitaevskii, *Electrodynamics of Continuous Media*, Butterworth-Heinemann, Oxford, UK, 1984.

[69] D. J. Jackson, *Classical Electrodynamics*, John Wiley & Sons, New York, NY, USA, 2nd edition, 1975.

[70] J. Smit and H. P. J. Wijn, *Ferrites*, Phlips Technical Library, Eindhoven, The Netherlands, 1975.

[71] N. Guskos, E. A. Anagnostakis, V. Likodimos, et al., "Ferromagnetic resonance and ac conductivity of a polymer composite of Fe_3O_4 and Fe_3C nanoparticles dispersed in a graphite matrix," *Journal of Applied Physics*, vol. 97, no. 2, Article ID 024304, 6 pages, 2005.